Canadian Science Publishing | Canadian Journal of Physics

Determination of the asymmetry term strength in the n − A elastic scattering process using a nonlocal optical model

Journal:	*Canadian Journal of Physics*
Manuscript ID	cjp-2020-0569.R1
Manuscript Type:	Article
Date Submitted by the Author:	18-Dec-2020
Complete List of Authors:	Sawalha , A.; The University of Jordan, Physics Department Jaghoub, M.I.; The University of Jordan, Physics
Keyword:	optical potential, nonlocality, angular distributions, nuclear reactions, nuclear structure
Is the invited manuscript for consideration in a Special Issue? :	Not applicable (regular submission)

Determination of the asymmetry term strength in the $n - A$ elastic scattering process using a nonlocal optical model

A. Sawalha and M. I. Jaghoub *

Physics Department, The University of Jordan, P.C. 11942, Amman, Jordan

January 28, 2021

Abstract

In previous works, the imaginary surface and (or) the imaginary volume depths of the optical potential were parametrised as linear functions of the projectile's incident energy and neutron-proton asymmetry $(N - Z)/A$ of the target nucleus. However, the obtained asymmetry strength parameters were not robust nor unique. In this work, we determine values for the strength parameters by simultaneously fitting 38 angular distribution data sets corresponding to neutron elastic scattering off chains of isotopes. For each isotopic chain, we considered the data sets that are measured at the same energy. This minimises the effect of the known energy dependence of the optical model and projects the dependence on the asymmetry term, which in turn leads to more reliable values of the strength parameters. To demonstrate the significance of the obtained strength values, we use the model to predict elastic angular distributions for neutron scattering off nuclei not considered in the χ^2 analysis. Our theoretical angular distributions are in good agreement with the measured data and are also comparable to the predictions of local global models. In addition, our predicted total elastic and total reaction cross sections are in fair overall agreement with experiment. An additional result of this work is the determination of a global set of nonlocal parameters that describe neutron elastic scattering off nuclei that fall in the mass range $24 \leq A \leq 208$ corresponding to incident neutron energies between $\approx 10 - 30$ MeV.

*E-mail address: mjaghoub@ju.edu.jo

1 Introduction

The conventional phenomenological optical model has been successfully used in describing the nucleon-nucleus scattering process [1] - [3]. One important aspect of the model is that it reduces the nucleon interaction with the complex many-body nuclear system into a simple two-body problem. However, the model's parameters are energy dependent, which is taken as a sign that the nucleon-nucleus scattering process is endowed with nonlocal effects [4]. The nonlocality in the optical potential is, partly, due to the fact that the underlying NN interaction is nonlocal and energy dependent. One source of nonlocality is a consequence of the Pauli exclusion principle, and is accounted for by antisymmetrizing the total wave function as in the Hartree-Fock theory [5]. In addition, in the Hartree-Fock equation, a spatially variable mass can be used to express the nonlocality due to exchange effects [6]. Coupling of the ground state to inelastic excitation channels is an important source of nonlocality. However, the large number of possible excitation channels renders the process of rigorously accounting for this nonlocality a very difficult task. Consequently, the effects of channel coupling on the scattering process are usually accounted for by numerically coupling the ground state to few, important low-lying exited states [7] and [8]. For example, the angular distributions corresponding to neutron scattering off a range of nuclei from ^{6}Li to ^{208}Pb were fitted using the phenomenological optical model with channel coupling (CC). The resulting potential parameters showed a noticeable reduction in their energy dependence [10]. In a more recent work, a semimicroscopic optical model with channel coupling was also used to fit the angular distributions and polarization data for neutron scattering off a range of nuclei falling in the mass range $12 < A < 208$. The real volume part of the potential was determined by folding the NN potential over the density of the nuclear target. The obtained parameters of the model showed a weak energy dependence compared to the case without channel coupling [11].

Another well known nonlocality is that proposed by Perey and Buck (PB) [9]. The nonlocal kernel of the potential was assumed to be separable into a potential form factor multiplied by a Gaussian nonlocality. The constant parameters of the model were determined by fitting the elastic angular distributions corresponding to neutron scattering off ^{208}Pb at 7.0 and 14.5 MeV. This nonlocal model successfully predicted the elastic angular distributions for neutron scattering off nuclei from ^{27}Al to ^{208}Pb over the 0.4 to 28 MeV energy range. In addition, the fixed parameters of the model were used to predict the elastic angular distributions for neutron scattering off nuclei ranging from aluminium to lead. A more recent source of nonlocality was proposed to be due to a change in the mass of the incident nucleon as a result of its interactions

with other nucleons inside the target nucleus [12]. The model reproduced the neutron elastic angular distributions off the light ^{12}C nucleus. Subsequent works showed the effectiveness of this velocity-dependent optical model (VDOM) in describing the elastic angular distributions corresponding to neutron and proton elastic angular off light $1p$-shell, intermediate and heavy nuclei. In addition, the model's predictions of the polarization data were in good overall agreement with the experimental data [13] - [15].

One might expect that the explicit inclusion of nonlocalities in the optical model may removes the energy dependence of the model's parameters. In fact, recent works have shown that although accounting for nonlocal effects in the optical model reduces the energy dependence of the parameters, this dependence was still needed to fine tune the elastic angular distribution fits [10] and [11]. In addition, Tian, Pang and Ma (TPM) used the nonlocal potential of Perey and Buck (PB) [9], which explicitly includes a Gaussian nonlocality, and fitted experimental angular distributions corresponding to nucleon elastic scattering off nuclei from ^{27}Al to ^{208}Pb within the 10 - 30 MeV energy range. Two fixed global sets of parameters were determined; one for protons and the other for neutrons [16]. In a subsequent work, investigation of neutron elastic scattering off intermediate and heavy nuclei (^{40}Ca, ^{90}Zr and ^{208}Pb) over the $\approx$ 5 - 40 MeV energy range, showed that the inclusion of a Gaussian nonlocality does not fully remove the energy dependence of the potential [17]. In fact, following the global model of Becchetti and Greenlees (BG) [2], Lovell *et. al.* expressed the imaginary surface depth (W_s) of the nonlocal potential as a linear function of energy and asymmetry $(N-Z)/A$, while the imaginary volume term (W_I) was expressed as a function of energy only:

$$W_I = a_1 E + c_1. \tag{1}$$

$$W_s = a_2 E + b_2 (N-Z)/A + c_2, \tag{2}$$

The five parameters a_i and b_i were simultaneously fitted to 24 neutron elastic angular distribution data sets. The potential parameters were initialized to those of PB values. Since the PB model does not contain an imaginary volume term, the TPM parameters were used for the imaginary volume term. This resulted in $b_2 = 0.74 \pm 0.46$ MeV, which is much smaller than the absolute value of 12 MeV of the BG global model. In addition, the relative error is clearly large. The χ^2 analysis was repeated but all the potential parameters were initialized to the values of TPM. This resulted in $b_2 = 4.5 \pm 0.5$ MeV, which is still smaller than the BG value. The authors showed that the inclusion of a Gaussian nonlocality does not fully remove the need for energy-dependent potential, but the asymmetry dependence is not robust nor unique. Although the considered nuclear targets cover a wide mass

and asymmetry ranges, the data sets did not constrain the value of the asymmetry parameter. A subsequent work considered proton elastic scattering off ^{40}Ca, ^{90}Zr and ^{208}Pb. But, in addition to the imaginary surface depth, the imaginary volume depth was also expressed as linear functions of energy and asymmetry as [18]:

$$W_I = a_1 E + b_1(N-Z)/A + c_1. \tag{3}$$

This resulted in more robust strength values for the asymmetry terms; namely $b_1 = 45.75 \pm 3.51$ MeV and $b_2 = 11.86 \pm 3.88$ MeV. Two more recent works also considered neutron [19] and proton [20] scattering off light $1p$-shell nuclei. For neutrons the resulting strength parameters for the asymmetry terms are $b_1 = -4.416 \pm 1.778$ MeV and $b_2 = 9.564 \pm 0.981$ MeV. The proton case was slightly more complicated. Two global sets of nonlocal parameters were needed to describe the elastic scattering data. One for the lower 10 - 39 MeV energy range for which $b_1 = 27.533 \pm 0.612$ MeV and $b_2 = 27.533 \pm 0.612$ MeV. While for the higher 40 - 70 MeV range, $b_1 = 41.766 \pm 3.002$ and $b_2 = 11.441 \pm 0.642$ all in units of MeV [20].

Clearly, the varied values of the asymmetry parameters b_1 and b_2 indicate the need for further analysis to determine more accurate values for the asymmetry strength parameters. Since each of the depths W_I and W_s is expressed as a linear function of energy and asymmetry, the energy dependence can easily mask the effect of the asymmetry term, which does not help in determining the values of strength parameters b_i. In this work our aim is to overcome this problem by considering neutron elastic scattering off long isotopic chains and, for each chain, fit the potential depths to angular distribution sets that are determined at the same (or nearly the same) energies. This should minimise the effect arising from the energy dependence of the potential depths while at the same time highlight the role played by the asymmetry term. All the experimental angular distribution sets considered in this work are taken from the EXFOR library [22].

Our analysis is based on the nonlocal model of Perey and Buck. The detailed derivation of the model is found in the PB paper [9]. Here we just present the integro-differential Schrödinger equation that corresponds to the PB nonlocal potential:

$$\left[\frac{\hbar^2}{2\mu}\nabla^2 + E\right]\Psi(\mathbf{r}) = -\left[(U_{so} + iW_{so})\, S(r)\mathbf{L}\cdot\sigma\right]\Psi(\mathbf{r}) + \int V(\mathbf{r},\mathbf{r}')\Psi(\mathbf{r}')d\mathbf{r}' + V_C(r)\Psi(\mathbf{r}), \tag{4}$$

where $V_C(r)$ is the coulomb potential, U_{so} and W_{so} are the depths of the local real and imaginary parts of the spin-orbit term and the form factor $S(r)$ is given by

$$S(r) = \left(\frac{\hbar}{m_\pi c}\right)^2 \frac{1}{a_{so} r}\exp\left(\frac{r-R_{so}}{a_{so}}\right)\left[1+\exp\left(\frac{r-R_{so}}{a_{so}}\right)\right]^{-2}. \tag{5}$$

The authors assumed the following separable form for the nonlocal kernel:

$$V(\mathbf{r},\mathbf{r}') = U(p)\frac{1}{\pi^{3/2}\beta^3}e^{-[\mathbf{r}-\mathbf{r}']^2/\beta^2}, \tag{6}$$

where β is a nonlocality parameter and

$$p = \frac{1}{2}|\mathbf{r}+\mathbf{r}'|, \tag{7}$$

while the form of $U(p)$ is similar to that adopted for local potentials; namely

$$-U(p) = V_R f_R(p) + iW_I f_I(p) + iW_s f_s(p), \tag{8}$$

with

$$f_j(p) = \left[1+\exp\left(\frac{p-R_j}{a_j}\right)\right]^{-1}, j = R \text{ or } I \tag{9}$$

and

$$f_s(p) = 4\exp\left(\frac{p-R_s}{a_s}\right)\left[1+\exp\left(\frac{p-R_s}{a_s}\right)\right]^{-2}, \tag{10}$$

where $R_i = r_i A^{1/3}$ (with $i = R, I,$ or s) and a_i are the nuclear mean radius and diffuseness parameters respectively.

Clearly, the PB nonlocal potential contains an imaginary volume and imaginary surface depths W_I and W_s. The imaginary parts of the optical model are known to account for the removal of flux from the elastic channel and, therefore, are related to nonlocal effects. This relation stems from the fact that nonlocality can be viewed as the removal of flux from the elastic channel at position $\mathbf{r_1}$, which reappears later at another position $\mathbf{r_2}$. For example, a neutron can be scattered out of the elastic channel at $\mathbf{r_1}$, then propagates to another position $\mathbf{r_2}$ where it is scattered back into the elastic channel by another interaction. The distance it travels from $\mathbf{r_1}$ to $\mathbf{r_2}$ is a measure of the distance over which the nonlocal effect is important. The nonlocality parameter β in equation (6) is a measure of this distance. The imaginary surface term accounts for absorption of incident flux at the nuclear surface and is mostly important at low energies. As the incident energy increases, the absorptive interactions that take place deeper within the nuclear volume acquire more importance. The $(N-Z)/A$ asymmetry dependence may arise from the isotopic spin dependence of the nucleon-nucleus interaction dependence which is proportional to $\pm\tau\cdot\mathbf{T}$, where τ is the isospin of the nucleon, while $\mathbf{T}$ is the isospin of the target nucleus. Further, the plus sign is for protons and the minus sign is for neutrons. This implies a sign change in the strength of the asymmetry term depending on the incident nucleon being a

proton or a neutron. The underlying NN interaction may also result in the presence of the asymmetry term in the optical model, and does not necessarily impose a strict sign change of the strength parameter depending on the type of the incident nucleon. The absence of the strength parameter sign change in the previous work of [17] to [20], and the present work is an evidence in support of the NN interaction giving rise to an asymmetry term in the nucleon-nucleus scattering process.

The PB nonlocal potential given in equation (6) contains one nonlocality parameter β , which is common to the real and imaginary parts of the potential. However, when the dispersive optical potential is extended to include nonlocal effects, leading to a nonlocal dispersive optical model, a nonlocality parameter is needed for each of the real and imaginary parts of the potential [23]. Furthermore, the values of the ranges of the nonlocality parameters are different from the value of $\beta = 0.85$ fm for the PB nonlocal potential.

2 Results and discussion

Table 1 shows the chains of isotopes used in the fitting procedure, the neutron incident energies and the references for the 50 angular distribution data sets that correspond to neutron elastic scattering off the 18 considered isotopes. For each isotopic chain we searched for experimental data sets which are measured at the same energies like, for example, the case for ^{54}Fe and ^{56}Fe isotopes. We also tried to do the same for elements belonging to different isotopic chains such as ^{24}Mg and ^{32}S at 14.8 MeV incident energy. This should help in highlighting the effect of the $(N - Z)/A$ asymmetry on the scattering process.

2.1 Individual energy fits

We have coupled the NLAT code [44] to SFRESCO [45] in order to fit the parameters of the nonlocal potential to the individual experimental angular distributions of Table 1. For consistency, in the χ^2 analysis, we always started from the TPM parameters. To reduce the number of the fit parameters, the same values of the radius (r_{so}) and diffuseness (a_{so}) were used for the real and imaginary parts of the spin-orbit interaction. The quality of each fit was judged visually and also qualitatively by calculating the χ^2 value per degree of freedom using the expression:

$$\chi^2_j = \frac{1}{N_j} \sum_{i=1}^{N_j} \left(\frac{(\frac{d\sigma(\theta_i)}{d\Omega})_{\rm theo} - (\frac{d\sigma(\theta_i)}{d\Omega})_{\rm exp}}{\Delta(\frac{d\sigma(\theta_i)}{d\Omega})} \right)^2 , \tag{11}$$

Table 1: List of nuclei , energies and experimental data references used in the fitting procedure. The $\chi^2_{\rm tot}$ values are also given.

Nucleus	Energy (MeV)	Reference	$\chi^2_{\rm tot}$	Nucleus	Energy (MeV)	Reference	$\chi^2_{\rm tot}$
^{24}Mg	14.8	[24]	1.970	^{60}Ni	14.7	[31]	
^{26}Mg	24	[25]	1.190		18.5	[35]	
^{32}S	14.8	[24]			24	[34]	1.749
	21.7	[26]	1.126	^{92}Mo	11	[36]	
^{34}S	21.7	[26]			20 , 26	[37]	2.316
	25.5	[26]	1.087	^{98}Mo	11	[38]	
^{40}Ca	11.9	[27]			20 , 26	[37]	2.801
	13.9	[28]		^{100}Mo	11 , 20 , 26	[37]	5.014
	16.9	[29]	0.936	^{116}Sn	11 , 24	[39]	1.185
^{48}Ca	11.9	[27]		^{118}Sn	11 , 24	[39]	
	16.8	[27]	1.542		14.9 , 18	[40]	1.779
^{54}Fe	11, 20, 26	[30]		^{124}Sn	11 , 24	[39]	0.665
	14.7	[31]	1.115	^{206}Pb	11	[38]	
^{56}Fe	11, 20, 26	[30]			13.7	[41]	
	14.7	[31]	1.096		21.6	[32]	3.322
^{58}Ni	14.7	[31]		^{208}Pb	11	[42]	
	16.9	[33]			13.7	[41]	
	24	[34]	1.014		20 , 22 , 24	[43]	4.635

where N_j is the number of degrees of freedom for data set j corresponding to a given incident proton energy, while $(\frac{d\sigma(\theta_i)}{d\Omega})_{\text{theo}}$ and $(\frac{d\sigma(\theta_i)}{d\Omega})_{\text{exp}}$ are the respective theoretical and experimental differential cross sections at angle θ_i, and $\Delta(\frac{d\sigma(\theta_i)}{d\Omega})$ is the corresponding experimental error. Furthermore, we calculated the total χ^2 value per degree of freedom (χ^2_{tot}) for each target nucleus, which we define as:

$$\chi^2_{\text{tot}} = \frac{\sum_j N_j \chi^2_j}{\sum_j N_j}, \tag{12}$$

where j runs over all the angular distribution data sets included in the fitting procedure for a given nucleus. In the χ^2 analysis of this work, an overall error of 10% was assumed for all data points of the differential cross sections. This is based on the assumption that systematic errors in the measurements is larger than the statistical errors typically included in the experimental papers [17].

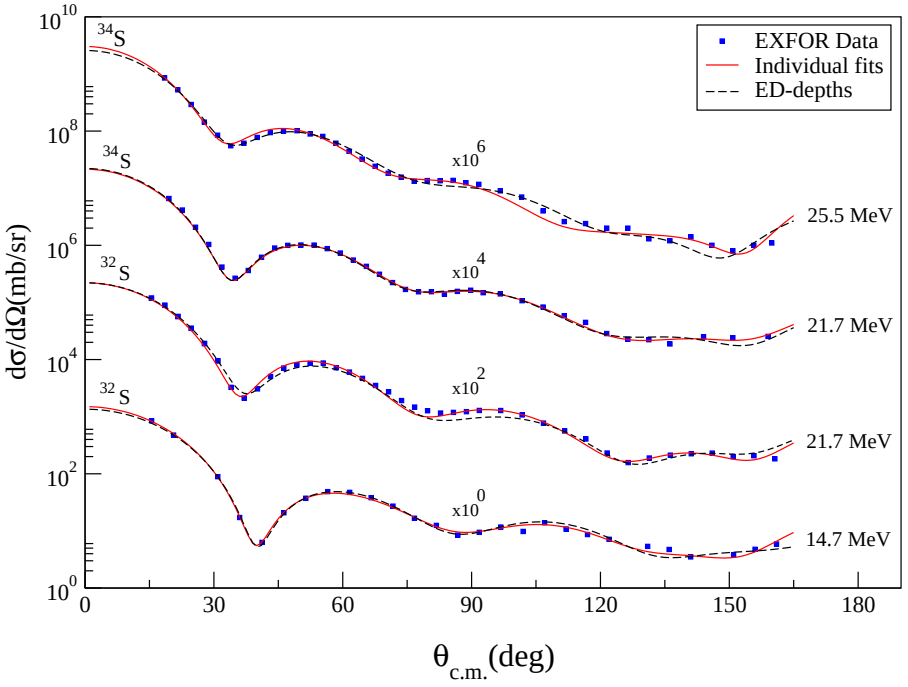

Figure 1: Best elastic angular distribution fits for neutron elastic scattering off ^{32}S and ^{34}S isotopes using the NLOMP. Solid curves are obtained by fitting the individual data sets. The dashed curves are obtained using the fixed geometrical parameters in Table 2 and the energy-dependent depths which are given by the expressions in Table 3.

Since we have fitted 50 data sets, including all the individual best fit parameters would lead to a lengthy manuscript. Instead, we have indicated the goodness of the fits by including the value of $\chi^2_{\rm tot}$ for each isotope as shown in Table 1. The low $\chi^2_{\rm tot}$ values indicate that the nonlocal model has reproduced the angular distributions well. The individual angular distribution fits for neutron elastic scattering off the sulphur, iron and lead isotopes are shown by the solid curves in Figs. 1 - 3. The good visual quality of the fits reflects the low $\chi^2_{\rm tot}$ values in Table 1.

3 Energy-dependent depths and fixed geometrical parameters

In this section we started from the TPM parameters and simultaneously fitted all the angular distributions belonging to each isotopic chain. This resulted in constant

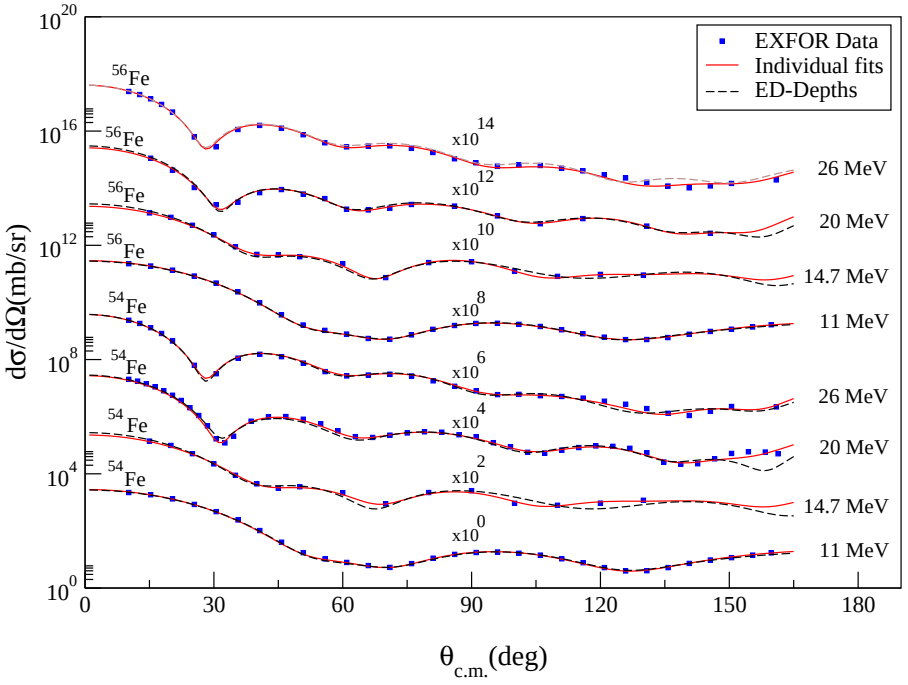

Figure 2: Best elastic angular distribution fits for neutron elastic scattering off ^{54}Fe and ^{56}Fe isotopes using the NLOMP. Solid curves are obtained by fitting the individual data sets. The dashed curves are obtained using the fixed geometrical parameters in Table 2 and the energy-dependent depths, which are given by the expressions in Table 3.

sets of parameters for each chain as shown in Table 2. The real volume depth V_R and the corresponding geometrical parameters r_R and a_R show the least variation with mass number A. However, the real and imaginary depths of the spin-orbit term show noticeable and less systematic variation with mass number. One way to reduce the energy dependence of the spin-orbit depths would be to fit polarization and angular distribution data simultaneously, but the NLAT code does not calculate the polarization observables.

Now we turn to investigating the energy dependence of the optical model parameters. Starting from the constant sets of parameters given in Table 2, we simultaneously fitted all the angular distributions of each isotopic chain. The geometrical parameters were fixed at their values, but the potential depths were allowed to vary with energy. The nonlocality parameter was fixed at its TPM value of $\beta = 0.9$ fm. Apart from the real and imaginary depths of the spin-orbit term, we found it possible

Table 2: Fixed nonlocal best fit parameters for neutron elastic scattering off each target nucleus. Starting from the TPM values the angular distributions for each isotopic chain were fitted simultaneously. The nonlocality parameter was fixed at its TPM value of $\beta = 0.9$ fm. The optical depths are in units of MeV, while the geometric parameters are in units of Fermi.

Parameters	Mg	S	Ca	Fe	Ni	Mo	Sn	Pb
V_R	70.453	70.500	71.031	71.400	71.597	72.130	73.468	73.701
r_R	1.214	1.296	1.273	1.259	1.262	1.238	1.236	1.226
a_R	0.680	0.614	0.635	0.597	0.606	0.698	0.679	0.700
W_I	2.962	2.929	1.023	3.203	1.124	2.969	3.125	3.120
r_I	1.002	1.400	1.184	1.000	1.300	1.300	1.000	1.000
a_I	0.400	0.600	0.600	0.600	0.600	0.400	0.593	0.401
W_s	20.457	21.002	18.475	18.193	20.331	22.605	21.607	15.539
r_s	1.132	1.209	1.248	1.172	1.160	1.205	1.202	1.192
a_s	0.507	0.414	0.480	0.480	0.452	0.460	0.447	0.518
V_{so}	6.771	4.061	10.530	7.515	5.010	8.674	4.277	4.907
W_{so}	-4.985	3.334	5.999	1.405	-1.384	-2.348	-4.592	-1.654
r_{so}	1.071	1.206	1.046	1.000	1.101	1.190	1.184	1.148
a_{so}	0.600	0.400	0.401	0.600	0.408	0.400	0.426	0.400
χ^2_{tot}	3.656	2.336	6.465	4.352	3.672	9.215	3.920	5.798

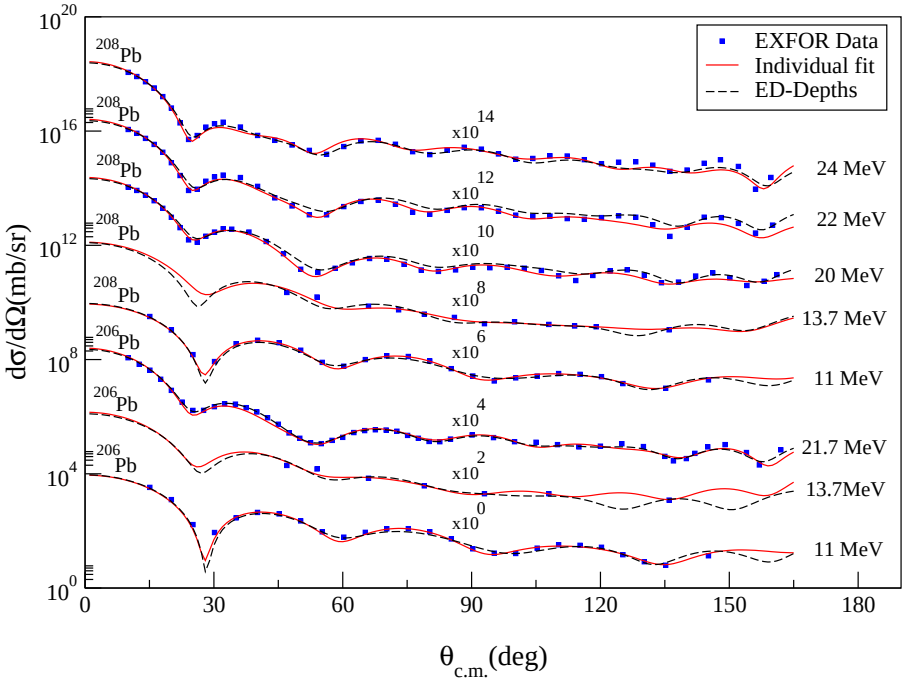

Figure 3: Best elastic angular distribution fits for neutron elastic scattering off ^{206}Pb and ^{208}Pb isotopes using the NLOMP. Solid curves are obtained by fitting the individual data sets. The dashed curves are obtained using the fixed geometrical parameters in Table 2 and the energy-dependent depths given by the expressions in Table 3.

to express the rest of the potential depths as linear functions of energy as can be seen in Table 3. Since all the data sets of each isotope were fitted simultaneously, the χ^2_{tot} values are slightly larger than the case for the individual fits. However, the corresponding best angular distribution fits shown by the dashed curves in Figs. 1 - 3 still show good agreement with the measured data. It is important to note here that the real volume depth V_R shows a weak energy dependence compared to the imaginary volume and imaginary surface depths. We shall return to this point in Section 3.2.

3.1 Global parameters

As we mentioned earlier, our primary goal is to determine reliable estimates of the strengths b_1 and b_2 of the asymmetry $(N-Z)/A$ term in the neutron-nucleus elastic scattering process. However, the linear energy dependence of W_I and W_s can

Table 3: The Energy-dependent depths parametrized as linear functions of energy. For each isotope we started from the fixed parameters of Table 2 and fitted the corresponding individual data sets of Table 1. The resulting depths were expressed as linear functions of energy. The geometrical and nonlocality parameters were not included in the fitting procedure.

Nucleus	Potential Depths (MeV)			χ^2_{tot}
	V_R	W_I	W_s	
^{32}S	-0.033E +72.02	0.25E - 0.76	-0.17E + 21.76	3.523
^{34}S	0.076E +70.05	0.66E - 13.78	-0.49E + 32.55	2.087
^{40}Ca	-0.049E +73.66	0.33E - 3.42	-0.39E + 21.62	1.886
^{48}Ca	0.028E + 69.12	0.49E - 5.28	-0.20E + 17.38	3.200
^{54}Fe	-0.029E +74.44	0.29E - 2.87	-0.36E + 28.11	3.825
^{56}Fe	-0.028E +72.85	0.24E + 0.18	-0.29E + 23.77	4.032
^{58}Ni	-0.031E +73.47	0.30E - 1.07	-0.18E + 19.32	3.135
^{60}Ni	0.018E +69.17	0.21E + 0.12	-0.29E + 24.15	2.771
^{92}Mo	0.008E +73.19	0.26E - 0.81	-0.29E + 23.92	6.434
^{98}Mo	-0.038E +72.78	0.17E + 0.62	-0.25E + 26.07	9.551
^{100}Mo	0.012E +69.07	0.27E - 1.76	-0.16E + 23.82	7.584
^{116}Sn	-0.020E +74.58	0.15E + 1.31	-0.14E + 23.68	3.316
^{118}Sn	-0.015E +75.06	0.29E - 3.04	-0.46E + 28.48	4.254
^{124}Sn	-0.021E +73.50	0.19E - 1.62	-0.17E + 22.94	2.313
^{206}Pb	0.081E +73.49	0.20E - 0.88	-0.27E + 18.93	8.531
^{208}Pb	0.056E +72.42	0.24E - 1.92	-0.08E + 18.83	6.534

easily mask the dependence on the $(N - Z)/A$ term. To minimize this effect and highlight the importance of the asymmetry term, for each isotopic chain, we considered angular distribution sets which are measured at the same neutron incident energies. Consequently, out of the 50 data sets of Table 1, we only included 38 sets in the fitting procedure as given in Table 4. Starting from the TPM parameters we simultaneously fitted all the 38 angular distribution data sets keeping the nonlocality parameter fixed at its TPM value of $\beta = 0.9$ fm. The resulting nonlocal, fixed set of global parameters is given in Table 5, which we shall refer to as the SJ set.

In reference [19], a fixed global set of parameters was obtained for neutron elastic scattering off light $1p$-shell nuclei. The imaginary volume term $W_I = 0.001$ MeV was obtained, which is much smaller than the value of 3.098 MeV of this work. This might reflect the fact that for light $1p$-shell nuclei, which mostly consist of diffuse edges, the surface interactions play a more prominent role than those that take place

Table 4: List of isotopic chains and the energies that correspond to the experimental angular distribution data sets which were included in the χ^2 analysis to determine the global nonlocal potential parameters of Tables 5 and Table 6.

Nucleus	Energy (MeV)	Nucleus	Energy (MeV)
^{24}Mg	24	^{92}Mo	11, 20, 26
^{32}S	21.7	^{98}Mo	11, 20, 26
^{34}S	21.7	^{100}Mo	11, 20, 26
^{40}Ca	11.9, 16.9	^{116}Sn	11, 24
^{48}Ca	11.9, 16.8	^{118}Sn	11, 24
^{54}Fe	14.7, 20, 26	^{124}Sn	11, 24
^{56}Fe	14.7, 20, 26	^{206}Pb	11, 13.7, 21.6
^{56}Ni	14.7, 24	^{208}Pb	11, 13.7, 22
^{60}Ni	14.7, 24		

Table 5: The SJ set of constant nonlocal parameters for neutron elastic scattering off intermediate and heavy nuclei. The values of the parameters were determined by fitting all the data sets of Table 1 simultaneously. The nonlocality parameter β was fixed at its TPM value of 0.9 fm. The potential depths are in units of MeV while the geometrical parameters are in units of Fermi.

V_R	r_R	a_R	W_I	r_I	a_I	W_s	r_s
72.840	1.245	0.646	3.098	1.000	0.700	19.664	1.182
a_s	V_{so}	W_{so}	r_{so}	a_{so}	β	χ^2_{tot}	
0.477	4.861	-1.606	1.165	0.303	0.900	10.733	

within the nuclear volume. However, the surface absorption depths W_s are similar for both cases, indicating the importance of inelastic surface interactions for light, intermediate and heavy nuclei. As can be seen in Table 5, the $\chi^2_{\rm tot}$ value for all the considered data sets is 10.733. In view of Eq. (12), this value indicates the small χ^2 values corresponding to the fits of the individual data sets, which in turn shows that the constant set of parameters reproduced the measured differential cross sections to a good extent. Visual inspection of the solid curves in Figs. 4 - 6 shows that even with an increased $\chi^2_{\rm tot}$ value, the measured data has been reproduced to a good extent.

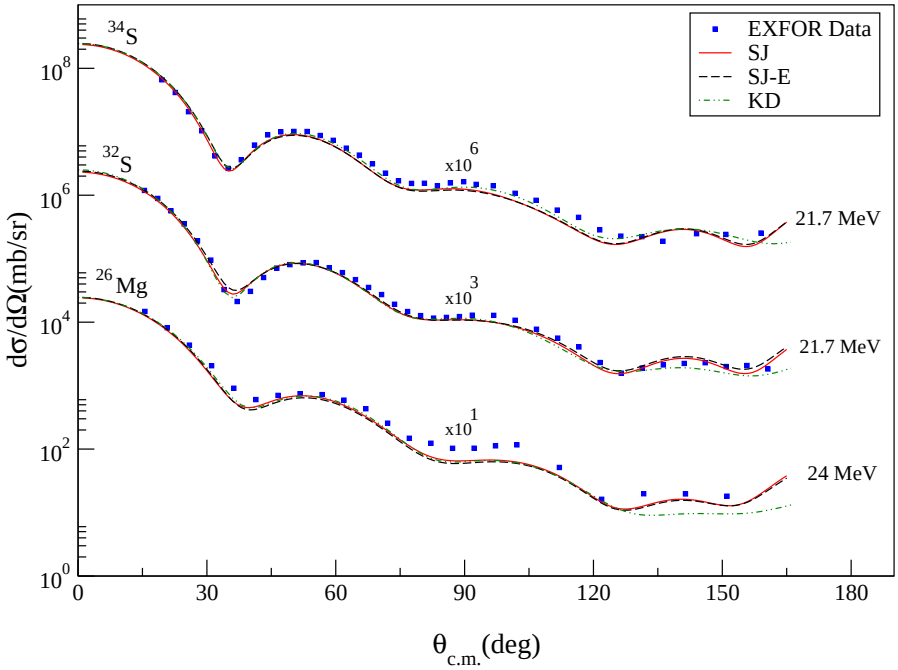

Figure 4: Best elastic angular distribution fits for neutron elastic scattering off ^{26}Mg, ^{32}S and ^{34}S nuclei using the NLOMP. Solid curves (SJ) are obtained using the global fixed parameters of Table 5. The dashed curves are obtained using the SJ-E set of parameters given in Table 6. Our best fits are compared to the dash-dotted curves (KD) which are obtained using the local optical model of reference [3].

3.2 Energy and asymmetry parametrization of the potential depths

Inspection of Table 3 shows that the energy dependence of the real volume depth V_R is at least an order of magnitude smaller than those for W_I and W_s. Therefore, we expressed it as a linear function of mass number A only by fitting the V_R values in Table 2 to a straight line according to:

$$V_R = 0.019A + 70.298, \tag{13}$$

while, following Refs. [18] - [20], the imaginary surface and volume depths were parametrized as linear functions of energy and the asymmetry as according to Eqs. (2) and (3). Using the above parametrizations and starting from the parameters of Table 5 we simultaneously fitted the 38 data sets of Table 4. Apart from V_R, W_I and W_s, the potential parameters were held fixed at their initial values while β was fixed

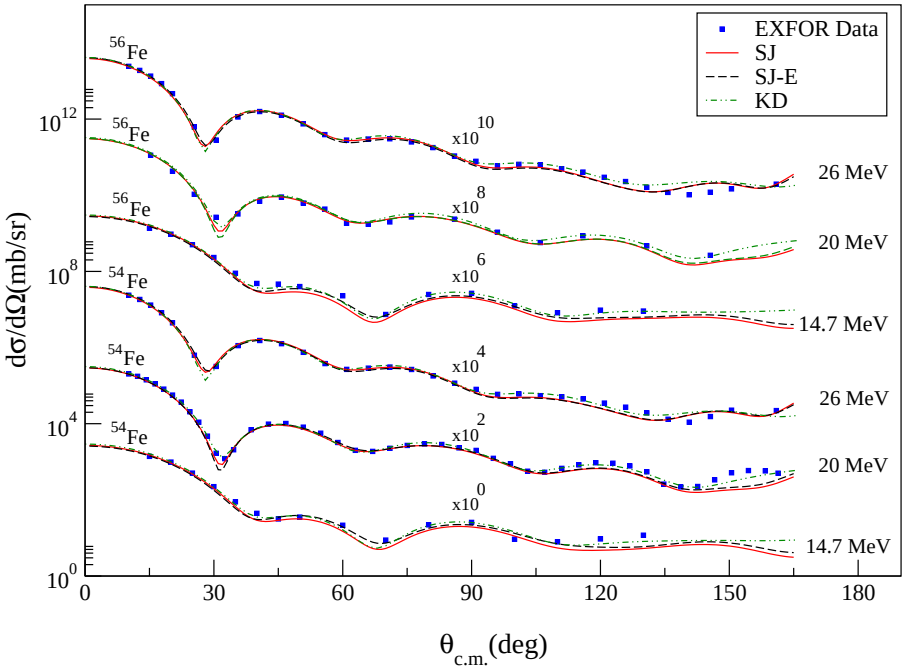

Figure 5: Best elastic angular distribution fits for neutron elastic scattering off ^{54}Fe and ^{56}Fe nuclei using the NLOMP. Solid curves (SJ) are obtained using the global fixed parameters of Table 5. The dashed curves are obtained using the SJ-E set of parameters given in Table 6. Our best fits are compared to the dash-dotted curves (KD) which are obtained using the local optical model of reference [3].

at its TPM value of 0.9 fm. The resulting best fit values for the a_i, b_i and c_i values are given in Table 6 and is referred to as the SJ-E set. Clearly, the value of $\chi^2_{\rm tot}$ is less than the case for the fixed global parameters of Table 5, which is expected as the W_s and W_I depths were allowed to become energy dependent. The corresponding best angular distribution fits are shown by the dashed curves in Figs. 4 - 6. Clearly, our fits are in good agreement with the measured data, and also with the predictions of the local global model of reference [3], which consists of energy and (or) asymmetry dependent depths and mass number dependent geometrical parameters.

In reference [17] only the surface absorption depth (W_s) was expressed as a linear function of both energy and the asymmetry term according to Eq. (2). Our value of $a_2 = 0.095 \pm 0.003$ indicates a noticeable reduction in the energy-dependence of W_s compared to the work of Lovell *et al.* who obtained a larger value of $a_2 = 0.200 \pm 0.004$. Our value is also smaller than value of 1.8220.005 obtained in Ref. [19]. We suggest this reduction to be due to our choice of the angular distribution data sets that were

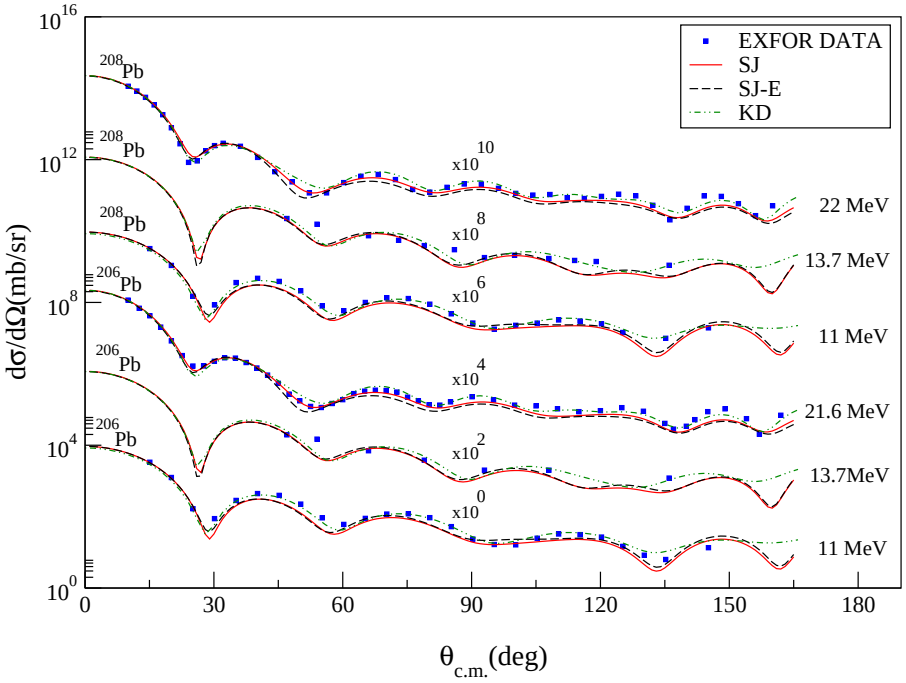

Figure 6: Best elastic angular distribution fits for neutron elastic scattering off ^{206}Pb and ^{208}Pb nuclei using the NLOMP. Solid curves (SJ) are obtained using the global fixed parameters of Table 5. The dashed curves are obtained using the SJ-E set of parameters given in Table 6. Our best fits are compared to the dash-dotted curves (KD) which are obtained using the local optical model of reference [3].

included in the χ^2 analysis. As shown in Table 4, for each isotopic chain the angular distributions for the different isotopes exist at the same energy. This reduces the effect of the change in energy and helps in better evaluation of the strength of the $(N-Z)/A$ asymmetry term . In this work, the dependence on the asymmetry term is more robust ($b_2 = 8.119 \pm 0.614$ MeV) compared to the value of $b_2 = 4.5 \pm 0.5$ MeV in Table II of reference [17]. It is worth noting that in the latter reference neutron scattering was only considered off three nuclei namely; ^{40}Ca, ^{90}Zr and ^{208}Pb. Although the three nuclei cover a wide range of asymmetry between the numbers of neutrons and protons, the effect of this term is masked by the dependence of W_s on energy. Although the structure of the $1p$-shell nuclei considered in [19] is different from the intermediate and heavy ones, the value of $b_2 = 9.564 \pm 0.981$ fm is close to our value. In the BG global local model [2], different parametrizations of the potential depths were used. All the depths V_R, W_I and W_s were expressed as linear

Table 6: The SJ-E set of best fit parameters obtained by fitting the angular distribution sets of Table 4. The potential parameters were initialized to the SJ values of Table 5. Only the imaginary surface (W_s) and imaginary volume (W_I) depths were allowed to vary according to equations (2) and (3). The nonlocality parameter was fixed at its TPM value of $\beta = 0.9$ fm.

a_1	b_1(MeV)	c_1(MeV)
0.250 ± 0.007	2.277 ± 0.193	-0.227 ± 0.107
a_2	b_2(MeV)	c_2(MeV)
0.095 ± 0.003	8.119 ± 0.614	15.746 ± 0.117
	β (fm)	χ^2_{tot}
	0.900	9.676

functions of energy, but only V_R and (or) W_s were assumed to have an asymmetry dependence. In addition, in one of the different parametrizations the radius a_I was taken to be mass number dependent. In the different parametrizations used, an absolute value of the strength parameter $b_2 = 12$ MeV was obtained. Despite the differences between the nonlocal model of this work and the local model of Becchetti and Greenlees both models have resulted in close values for the absolute value of the asymmetry strength parameter b_2.

4 Predictions of the global nonlocal model

Although our main aim has been to obtain a better estimate of the strength parameters b_i of the asymmetry term, here we shall investigate the effectiveness of our determined fixed (SJ) and energy-dependent (SJ-E) nonlocal global parameters in predicting the elastic angular distributions and total cross sections which were not included in the fitting procedure. The agreement of such predictions with the measured data should indicate how robust the model is, and in turn, indicates the accuracy of the determined strength parameters. We used the SJ and SJ-E sets given in Tables 5 and 6 to predict the differential cross sections corresponding to neutron elastic scattering off ^{28}Si and ^{90}Zr. The predicted angular distributions are compared to the measured data in Fig. 7, while the neutron incident energies and the corresponding individual and total χ^2 values per degree of freedom are given in Table 7. Clearly, our predictions are in very good agreement with the measured data and compare well to those obtained by the global local model of Konning and Delaroche, where the potential depths were parametrized in terms energy and (or) asymmetry while the geometrical parameters were expressed in terms of mass number [3]. Inspecting

Table 7 shows that the $\chi^2_{\rm tot}$ values corresponding to the energy-dependent SJ-E set are smaller than those corresponding to the fixed SJ set of parameters. This asserts the conclusions of previous works that the explicitly inclusion of nonlocality in the optical model does not fully remove the need for energy-dependent potential depths.

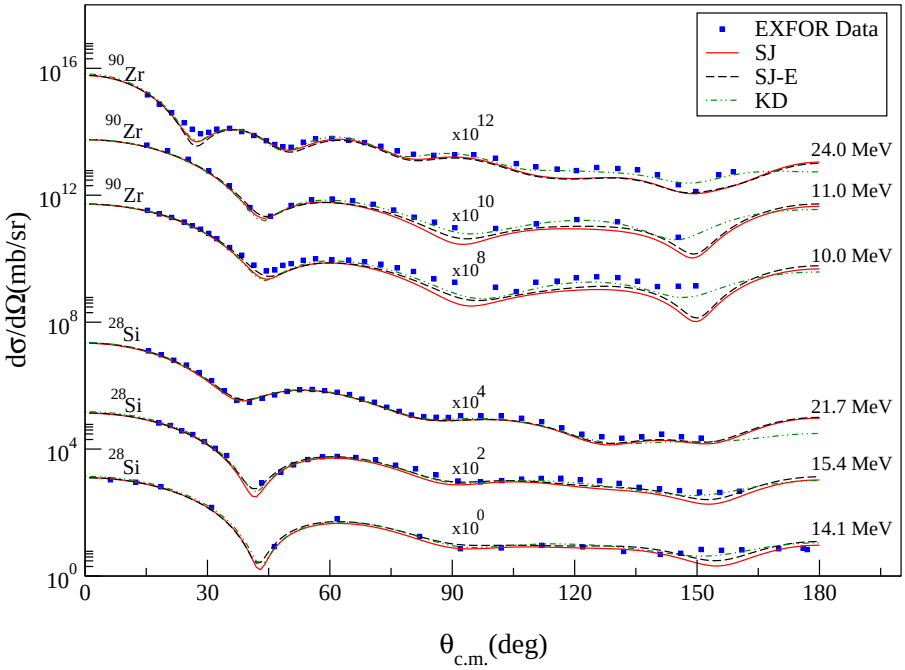

Figure 7: Predicted elastic angular distribution for neutron elastic scattering off ^{28}Si and ^{90}Zr. Solid curves (SJ) are obtained using the global fixed parameters of Table 5. The dashed curves (SJ-E) correspond to the fixed geometrical parameters in Table 2 and the energy-dependent depths which are given by the expressions in Table 6. Our predictions are compared to the dash-dotted curves (KD) which are obtained using the local optical model of reference [3]. The angular distributions are taken from references [26], [36] and [46] - [47] .

Now we turn to the calculations of the total cross sections. Since the NLAT code [44] does not calculate the total cross section, we calculated the required total elastic (σ_{el}) and total reaction (σ_r) cross sections using the following expressions [51]:

$$\sigma_{el} = \frac{\pi}{k^2} \sum_l \left[(l+1)|e^{2i\delta_{l+}} - 1|^2 + l|e^{2i\delta_{l-}} - 1|^2 \right], \tag{14}$$

and

$$\sigma_r = \frac{\pi}{k^2} \sum_l \left[(2l+1) - (l+1)|e^{2i\delta_{l+}}|^2 - l|e^{2i\delta_{l-}}|^2 \right], \tag{15}$$

where δ_{l+} and δ_{l-} are the scattering phase shifts corresponding to total angular momentum quantum numbers $j = l + 1/2$ and $j = l - 1/2$, respectively, for all the partial waves that contribute in the scattering process. Clearly, the total cross

Table 7: The individual and total χ^2 values per degree of freedom for the predicted distribution fits corresponding to elastic neutron scattering off ^{28}Si and ^{90}Zr.The experimental data are taken from references [26], [36] and [46] - [47]

Nucleus	E (MeV)	χ^2		$\chi^2_{\rm tot}$	
		SJ	SJ-E	SJ	SJ-E
^{28}Si	14.1	8.551	10.625		
	15.4	8.346	3.585		
	21.7	3.777	2.942	6.454	4.843
^{90}Zr	10	20.802	15.031		
	11	12.538	7.409		
	24	11.066	13.698	15.039	12.822

section σ_{tot} is the sum of the total elastic and total reaction cross sections. Since not many measured total cross sections are available in the EXFOR library, in Figs. 8 to 10, we compare our theoretical values to the experimental values in addition to evaluated cross sections which are available in the ENDF (Evaluated Nuclear Data File) library [49]. Inspection of the figures shows that our predictions are in good overall agreement with the experimental values and with those of other models. The good predictions for the elastic angular distributions and total cross sections is an indication that our determined values for the asymmetry strength parameters b_i of equations (2) and (3) are reliable.

5 Conclusion

In this work we have determined the values of the asymmetry $(N-Z)/A$ strength parameters by simultaneously fitting 38 elastic angular distribution sets that correspond to neutron elastic scattering off chains of isotopes. The imaginary surface (W_s) and imaginary volume (W_I) depths were expressed as linear functions of energy and asymmetry according to equations (2) and (3) respectively. To obtain reliable estimates of the strength parameters b_1 and b_2 we considered data sets which are measured at the same energy as shown in Table 4. This minimises the effect of the energy dependence on the scattering process and, at the same time, projects the effect of the asymmetry term. Our value $b_2 = 8.119 \pm 0.614$, for the asymmetry strength of the imaginary surface depth, is more robust than the corresponding values of 0.74 ± 0.46 and 4.5 ± 0.5 MeV obtained in reference [17]. Furthermore, neutron elastic scattering off light $1p$-shell nuclei using the nonlocal model of PB was consid-

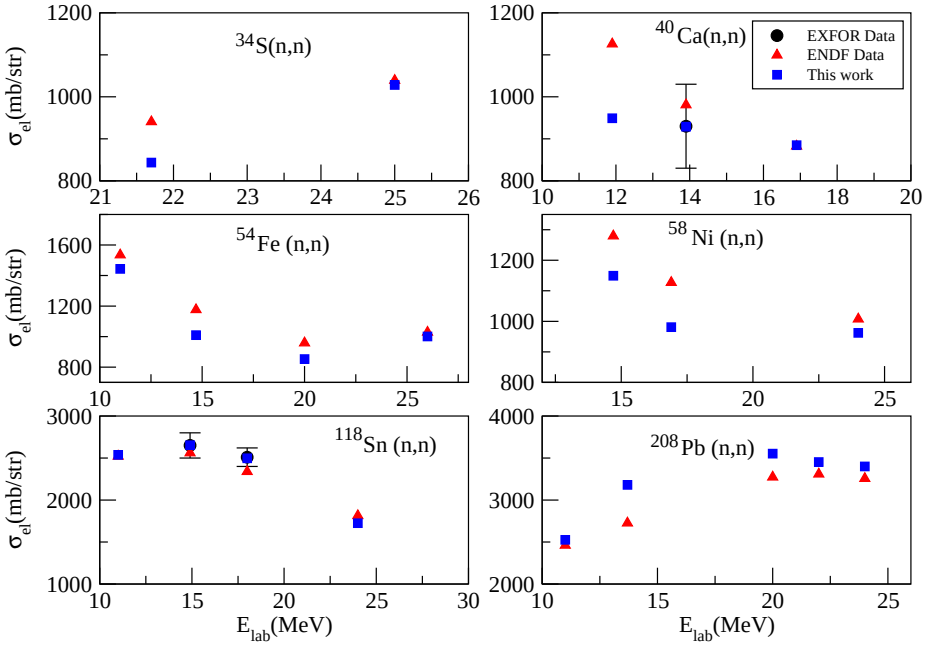

Figure 8: Predicted total elastic cross sections for neutron elastic scattering off a range of nuclei using the individual fit parameters of the nonlocal model. The total elastic cross sections are taken from references [48] - [49] presented in the EXFOR and the ENDF (Evaluated Nuclear Data File).

ered in reference [19] and resulted in $b_1 = -4.416 \pm 1.778$ MeV and $b_2 = 9.564 \pm 0.981$ MeV. Although the structure of such light nuclei is different from the intermediate and heavy ones considered in this work, the values of b_2 are close, but our value $b_1 = 2.277 \pm 0.193$ is different and of opposite sign. In the local model of Becchetti and Greenlees [2], the absolute value of the strength of the imaginary surface term is 12.0 MeV, which is close to our obtained value but the sign is different. The BG model is based on a local optical model, while we employed the nonlocal model of Perey and Buck with a Gaussian nonlocality. The different natures of the two models might explain the opposite signs of the strength parameters b_2. In fact, in the BG work, the strength parameter b_2 was assumed to be a consequence of isotopic dependence of the form $\tau \cdot \mathbf{T}$ where τ is the isospin of the incident neutron, while $\mathbf{T}$ is the isospin of the target nucleus. This leads to a negative value of b_2 for neutrons. In fact, the asymmetry dependence in the optical potential may also arise from the underlying NN interaction which is folded over the density of the nuclear target to deduce the optical model potential terms. This does not necessarily introduce a sign

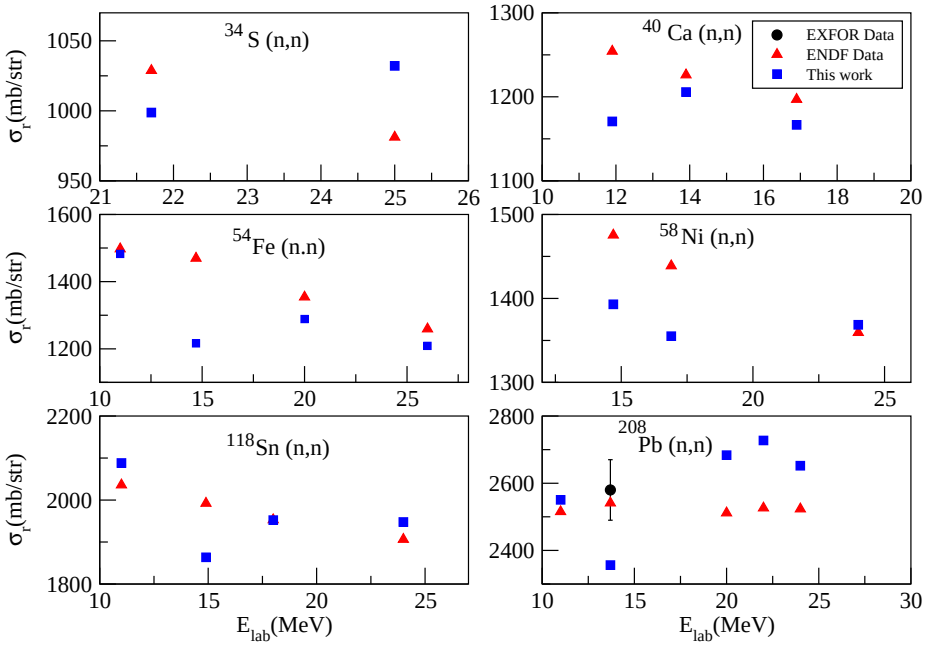

Figure 9: Predicted total reaction cross sections for neutron elastic scattering off a range of nuclei using the individual fit parameters of the nonlocal model. The reaction cross sections are taken from reference [50].

difference depending on the incident particle being a proton or a neutron.

A successful optical model is judged by its ability to predict physical observables. As a test of the effectiveness of the nonlocal model of this work, we used our parameter sets to predict elastic differential cross sections for energies and nuclei not considered in the fitting procedure. The resulting theoretical angular distributions are in good agreement with the measured data as can be seen in Fig. 8 and the low χ^2 and $\chi^2_{\rm tot}$ values of Table 7. Our predicted angular distributions are also comparable to those of the local global KD model [3]. We also predicted total elastic and reaction cross sections, which are in fair overall agreement with the experimental data as can be seen in Fig. 9. The agreement of our predictions with the measured values is an indication of the reliability of the determined potential parameters and the asymmetry strengths.

Finally, an additional consequence of the χ^2 analysis considered in this work is the determination of a global set of nonlocal parameters for neutron elastic scattering off intermediate and heavy nuclei falling in the mass range $24 \leq A \leq 208$.

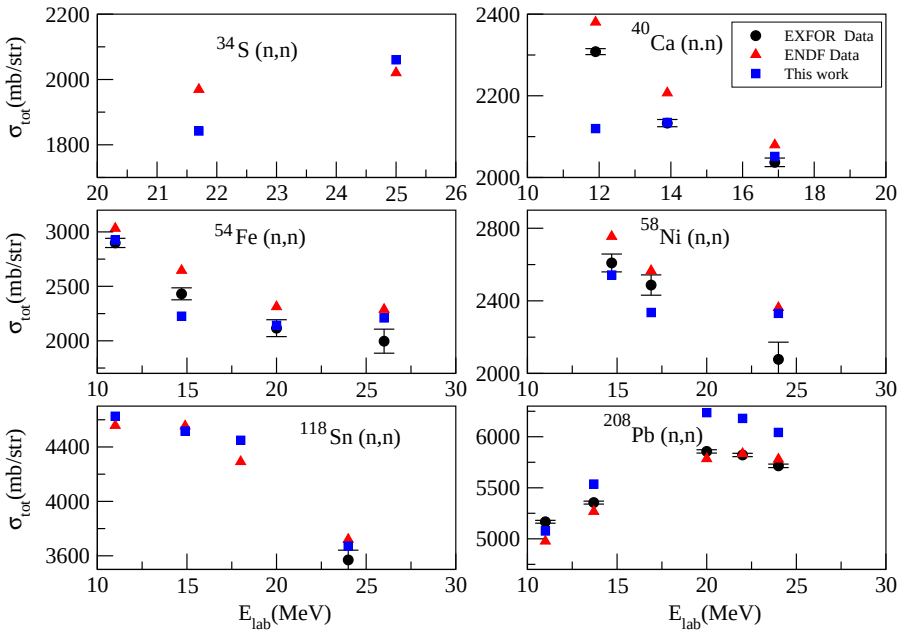

Figure 10: Predicted total cross sections for neutron elastic scattering off a range of nuclei using the individual fit parameters of the nonlocal model. The reaction cross sections are taken from reference [50].

Acknowledgement
We thank the Deanship of Scientific Research at the University of Jordan for funding this research work.

References

[1] J. H. Dave and C. R. Gould, Physical Review C bf 28, 2212 (1983).

[2] F. D. Becchetti and G. W. Greenlees, Physical Review **182**, 1190 (1969).

[3] A.J. Koning, J.P. Delaroche, Nuclear Physics A **713**, 231 (2003).

[4] P. Fraser, K. Amos, S. Karataglidis, L. Canton, G. Pisent, J.P. Svenne, European Physical Journal A **35**, 69 (2008).

[5] N. Austern, Physical Review **137**, 752 (1965).

[6] P. Ring, P. Schuk, The Nuclear Many-Body Problem, 1st edition, Springer-Verlag, 1980, p. 212.

[7] E. Cereda, M. Pignanelli, S. Micheletti, H.V. von Geramb, M.N. Harakeh, R. De Leo, G. DErasmo, A. Pantaleo, Physical Review C **26, 1941 (1982).**

[8] G. H. Rawitscher, Nuclear Physics A **475, 519 (1987).**

[9] F. Perey and B. Buck, Nucl. Phys. **32**, 353 (1962).

[10] W. S. Al-Rayashi and M. I. Jaghoub, Physical Review C **93**, 064311 (2016).

[11] S.B. Masadeh, M.I. Jaghoub, Physical Review C **100**, 014603 (2019).

[12] M. I. Jaghoub, M. F. Hassan and G. H. Rawitscher, Physical Review C **84**, 034618 (2011) .

[13] M. I. Jaghoub, Phys. Rev. C **85**, 024606 (2012).

[14] R.A. Zureikat, M.I. Jaghoub , Nucl. Phys. A **916**, 183 (2013).

[15] I. N. Ghabar and M. I. Jaghoub, Physical Review C **91**, 064308 (2015).

[16] Y. Tian, D.-Y. Pang, and Z.-Y. Ma, International Journal of Modern Physics E **24**, 1550006 (2015).

[17] A. E. Lovell, P.-L. Bacq, P. Capel, F. M. Nunes, and L. J. Titus, Physical Review C 96, 051601(R) (2017).

[18] M. I. Jaghoub, A. E. Lovell and F. M. Nunes, Physical Review C **98**, 024609 (2018).

[19] T. Aqel and M. I. Jaghoub , Nuclear Physics A **989**, 145 (2019).

[20] T. Aqel and M. I. Jaghoub , European Physical Journal A **56**, 216 (2020).

[21] R. Varner, W. Thompson, T. McAbee, E. Ludwig, and T. Clegg, Physics Reports **201**, 57 (1991).

[22] N.Otuka, E.Dupont, V.Semkova, B.Pritychenko, A.I.Blokhin, M.Aikawa, S.Babykina, M.Bossant, G.Chen, S.Dunaeva, R.A.Forrest, T.Fukahori, N.Furutachi, S.Ganesan, Z.Ge, O.O.Gritzay, M.Herman, S.Hlava, K.Kat, B.Lalremruata, Y.O.Lee, A.Makinaga, K.Matsumoto, M.Mikhaylyukova, G.Pikulina, V.G.Pronyaev, A.Saxena, O.Schwerer, S.P.Simakov, N.Soppera, R.Suzuki, S.Takcs, X.Tao, S.Taova, F.Trknyi, V.V.Varlamov, J.Wang, S.C.Yang, V.Zerkin, Y.Zhuang, "Towards a More Complete and Accurate Experimental Nuclear Reaction Data Library (EXFOR): International Collaboration Between Nuclear Reaction Data Centres (NRDC)", Nucl. Data Sheets **120**, 272 (2014).

[23] H. Mahzoon, M. J. Charity, R. H. Dickhoff, W. H. Dussan, and S. J. Waldecker, Physical Review Letters **112**, 162503 (2014).

[24] Centre dÉtudes Nucleaires, Saclay Reports, No.5144 (1981).

[25] R.C. Tailor, J. Rapaport, R.W. Finlay, G. Randers-Pehrson , Nucl. Phys. A **401**, 237 (1983).

[26] R. Alarcon, J. Rapaport, Nucl. Phys. A **458**, 502 (1986).

[27] J.M. Mueller, R.J. Charity, R.Shane, L.G. Sobotka, S.J. Waldecker, W.H. Dickhoff, A.S. Crowell, J.H. Esterline, B. Fallin, C.R. Howell, C. Westerfeldt, M. Youngs, B.J. Crowe, III, R.S. Pedroni , Phys. Rev. C **83**, 064605 (2011)

[28] W. Tornow, E. Woye, G.Mack, C.E.Floyd, K.Murphy, P.P.Guss, S.A.Wender, R.C.Byrd, R.L.Walter, T.B.Clegg, H.Leeb , Nucl.Phys. A **385**, 373 (1982)

[29] G.M.Honore, W. Tornow, C.R.Howell, R.S.Pedroni, R.C.Byrd, R.L.Walter, J.P.Delaroche , Phys. Rev. C **33**, 1129 (1986).

[30] S. Mellema, R.W.Finlay, F.S. Dietrich, F. Petrovich , Phys. Rev. C **28**, 2267 (1983).

[31] A.I.Tutubalin, A.P.Klyucharev, V.P.Bozhko, V.Ya.Golovnya, G.P.Dolya, A.S.Kachan, N.A.Shlyakhov, Conf: 2.Conf.on Neutron Physics, Kiev, Vol.3, 62 (1973).

[32] N. Olsson , B. Trostell, E. Ramström, B. Holmqvist and F. S. Dietrich Nuclear, Physics A **472**, 237 (1987).

[33] R.S. Pedroni, C.R. Howell, G.M. Honore, H.G. Pfutzner, R.C. Byrd, R.L. Walter, J.P. Delaroche, Phys. Rev. C **38**, 2052 (1988).

[34] Y. Yamanouti, J. Rapaport, S.M. Grimes, V. Kulkarni, R.W. Finlay, D. Bainum, P. Grabmayr, G. Randers-Pehrson , Conference on Nuclear Cross Sections.

[35] Y. Yamanouti, M. Sugimoto, S. Chiba, M. Mizumoto, K. Hasegawa, Y. Watanabe Conf.on Nucl. Data for Sci.and Technol.,Juelich 1991, 717 (1991).

[36] D.E.Bainum, R.W.Finlay, J.Rapaport, M.H.Hadizadeh, J.D.Carlson, J.R.Comfort , Nucl. Phys. A **311**, 492 (1978).

[37] J.Rapaport, T.S.Cheema, D.E.Bainum, R.W.Finlay, J.D.Carlson , Nucl. Phys. A **313**, 1 (1979).

[38] J.C. Ferrer, J.D. Carlson, J. Rapaport , Nucl. Phys. A **275**, 325 (1977)

[39] J. Rapaport, M. Mirzaa, M. Hadizadeh, D.E. Bainum, R.W. Finlay , Nucl. Phys. A **341**,56 (1980).

[40] S. Chiba, Y. Yamanouti, M. Sugimoto, M. Mizumoto, Y. Furuta, M. Hyakutake, S. Iwasaki , Jour. of Nuclear Science and Technology, Vol.25, 511 (1988).

[41] G.E.Belovitskii , L.N.Kolesnikova , I.M.Frank , Soviet Journal of Nuclear Physics, Vol.15, 369 (1972).

[42] J. Rapaport, T.S. Cheema, D.E. Bainum, R.W. Finlay, J.D. Carlson , Nucl. Phys. A **296**, 95 (1978).

[43] R.W. Finlay, J.R.M. Annand, T.S. Cheema, J. Rapaport, F.S. Dietrich , Phys. Rev.C **30**, 796 (1984).

[44] L. Titus, A. Ross, and F. Nunes, Computer Physics Communications **207**, 499 (2016).

[45] I. J. Thompson, Computer Physics Reports **7**, 167 (1988).

[46] M. A. Al-Ohali, J.P. Delaroche, C.R. Howell, M.M. Nagadi, A.A.Naqvi, W.Tornow, R.L.Walter, G.J.Weisel, Physical Review C **86**, 034603 (2012).

[47] Y.Wang, J.Rapaport, Nuclear Physics A **517**, 301 (1990).

[48] W. J. McDonald, J. M. Robson, Nuclear Physics **59**, 321 (1964).

[49] A.J. Koning, D. Rochman, J.-Ch. Sublet, N. Dzysiuk, M. Fleming, and S. van der Marck, TENDL: Complete nuclear data library for innovative nuclear science and technology, Nuclear Data Sheets **155**, 1 (2019).

[50] G.M.Haas, P.L.Okhuysen, Physical Review **132**, 1211 (1963).

[51] C. J. Joachain, *Quantum Scattering theory*, North-Holland Publishing Company, p. 502, 1975.